Journal of Alloys and Compounds 645 (2015) S56–S60

Contents lists available at ScienceDirect

Journal of Alloys and Compounds

journal homepage: www.elsevier.com/locate/jalcom

Amorphous Zr-based thin films fabricated by magnetron sputtering for potential application in hydrogen purification

Shahrouz Nayebossadri *, Daniel Smith, John Speight, David Book

School of Metallurgy and Materials, University of Birmingham, Edgbaston, Birmingham B15 2TT, UK

ARTICLE INFO

Article history:
Available online 11 February 2015

Keywords:
Hydrogen purification
Metallic membranes
Amorphous alloys
Thin films
Zr-based alloys
Magnetron sputtering

ABSTRACT

Amorphous hydrogen separation membranes are under development because of their resistance to hydrogen embrittlement, improved mechanical properties, resistance to corrosion and most importantly lower intrinsic cost. The Closed Field Unbalanced Magnetron Sputter Ion Plating (CFUBMSIP) is a versatile technique for deposition of high quality thin-films of almost any composition, while enabling the control of film size, thickness and shape. In this work, it was demonstrated that thin-films (~3–6 μm) of amorphous $Zr_{40.5}Ni_{59.5}$, $Zr_{54}Cu_{46}$ and $Zr_{30}Cu_{57.5}Y_{12.5}$ could be deposited onto glass substrates by the CFUBMSIP technique. XRD measurements only showed one broad peak for each alloy, with a peak centred between 36° and 42° 2θ, indicating that the films were amorphous. Surface analysis by SEM and confocal microscopy suggest deposition of continuous films. The thermal stability of the films appears to be mainly governed by the alloying elements and their compositions. However, the measured activation energies indicated that the nucleation and growth mechanism in the magnetron sputtered films may be different from that reported for melt-spun amorphous alloys with similar compositions.

1. Introduction

Palladium and Pd alloy membranes are currently used for hydrogen purification [1]. However, the cost of Pd membranes is considered to be prohibitively expensive for large-scale hydrogen purification applications [2]. The cost of Pd membranes in combination with their susceptibility to hydrogen embrittlement [3] and susceptibility to surface poisoning by impurity gases such as CO_2, CO and H_2S [4,5] has motivated the investigation of alternative materials for hydrogen separation membranes. The use of amorphous materials for hydrogen separation membrane can address several problems associated with the use of crystalline materials such as hydrogen embrittlement and high cost [6]. Some of the amorphous zirconium-based membranes, and in particular $Zr_{36}Ni_{64}$, $Zr_{54}Cu_{46}$, and $Zr_{30}Cu_{60}Y_{10}$ alloys, have been shown by computational [7,8] and experimental studies [9,10] to have hydrogen permeability values close to that of Pd.

Amorphous metal membranes can be produced by melt spinning, whereby molten metal is rapidly quenched onto a spinning copper wheel resulting in a metal ribbon in which non-equilibrium microstructures can effectively be captured [11]. Numerous examples of amorphous ribbons, such as $Zr_{54}Cu_{46}$ (30–40 μm thickness) [12] and ternary Ni–Nb–Zr films [13,14] were fabricated by melt spinning for hydrogen separation membranes. However, this technique imposes certain restrictions on possible alloy compositions, as incorporation of higher melting point elements may exceed the upper temperature limit that can be experimentally achieved [8]. In addition, precise control of the shape and size of the melt spun ribbons is difficult. Maintaining a uniform ribbon thickness with desired materials properties depend on the strict control of the process parameters, such as flow of molten metal and solidification rate [15]. The morphology of the output ribbon also strongly depends on the ribbon solidification time [15].

Alternatively, a physical vapour deposition (PVD) method can be used, as reported for the fabrication of amorphous Zr–Ni [16] and Zr–Cu [17,18] thin films. PVD techniques, such as magnetron sputtering, may allow the rapid and convenient production of an amorphous membrane over a wider compositional range (compared to melt spinning), while enabling good control of the film size, shape, and thickness. The Closed Field Unbalanced Magnetron Sputter Ion Plating (CFUBMSIP) uses a high density of low energy bombarding ions for production of very dense films with relatively low internal stresses [19]. In addition, the use of low bias voltage on the work piece allows the deposition of films at a low temperature, which could be beneficial when attempting to produce amorphous alloys. This work will investigate the possibility of using this particular type of magnetron sputtering, (CFUMSIP)

* Corresponding author. Tel.: +44 (0) 121 414 5213.
E-mail address: s.nayebossadri@bham.ac.uk (S. Nayebossadri).

http://dx.doi.org/10.1016/j.jallcom.2015.01.230
0925-8388/

[19], to fabricate thin amorphous films of $Zr_{36}Ni_{64}$, $Zr_{54}Cu_{46}$, and $Zr_{30}Cu_{60}Y_{10}$ alloys, due to their comparable hydrogen permeability to Pd [7–10]. Structure, composition, surface morphology and thermal stability of the alloys will be assessed.

2. Materials and method

Zirconium, copper, nickel and yttrium sputtering targets (99.9% purity) were obtained from Teer Coatings Ltd. Films with varying thicknesses were deposited onto 76 × 26 mm glass microscope slides (Thermo Scientific) by the Closed Field Unbalanced Magnetron Sputter Ion Plating (UPD 350-4), and were then peeled off, as shown in Fig. 1. (These films would require support in order to be used as hydrogen separation membranes.) The optimum sputtering conditions to produce the desired $Zr_{36}Ni_{64}$, $Zr_{54}Cu_{46}$ and $Zr_{30}Cu_{60}Y_{10}$ amorphous films, were obtained via a series of 10 min test coatings in which the Zr target current was varied, and the other sputtering parameters were fixed. The final sputtering conditions for each film deposition is given in Table 1. Relatively low target currents were selected, which seemed to be necessary to avoid crystallisation. The sputtering chamber was evacuated to approximately 10^{-6} mbar prior to the depositions and refilled to ~2.5×10^{-3} mbar with continuous flow (25 ml/min) of ultra-high purity argon during the deposition runs. A bias voltage of 50 V was applied to each magnetron during deposition runs. Final samples were deposited using pulsed DC, with a constant target to substrate distance and a sample rotation speed of 5 rpm, for approximately 3 h (18 runs of 10 min each). The cooling period between each run was designed to avoid sample overheating and possible crystallisation during the deposition process.

X-ray Diffraction (XRD) measurements of the films were performed using a Bruker D8-Advanced diffractometer with monochromatic Cu Kα radiation (λ = 1.54056 Å). The surface morphology and atomic compositions were analysed by a Joel 6060 Scanning Electron Microscope (SEM) equipped with an INCA 300 Energy Dispersive Spectrometer (EDS). The surface roughness and films thicknesses were examined using an Olympus LEXT OLS 3100 mounted on a Table Stable anti-vibration mounting. The system uses a 408 nm Class II ultraviolet laser source and has a planar resolution (X and Y) of 120 nm and a spatial pattern (Z resolution) of 10 nm. A part of the glass substrate was masked by Kapton tape, which was removed after the deposition, allowing step height film measurements.

Differential Scanning Calorimetry (DSC) measurements were performed on films that had been peeled-off of their glass substrates, under 3 bar Ar (flowing at 100 ml min^{-1}) using a Netzsch DSC204HP system at heating rates of 2, 5, 10, 15, and 20 °C min^{-1}.

3. Results and discussion

3.1. Structural and compositional characterisation

The X-ray diffraction patterns of Zr-based alloys after deposition are given in Fig. 2. Zr–Ni, and Zr–Cu–Y alloys show common characteristic of amorphous materials with a broad XRD peak between 30° and 50°. A similar broad peak can be also observed for the Zr–Cu alloy, with splits in the peak possibly suggesting some phase segregation or the formation of a small amount of nano-crystalline phase (Fig. 1b). Similarly, broad XRD peaks at around $2\theta = 40°$ were also observed for $Zr_{36}Ni_{64}$ and $Zr_{54}Cu_{46}$ alloys fabricated by melt spinning [12,9]. Hence, the XRD patterns in Fig. 1 indicate that it is possible to fabricate amorphous and nano-crystalline thin-film membranes of Zr–Ni, Zr–Cu, and Zr–Cu–Y by magnetron sputtering once deposition conditions are accurately defined to avoid crystallisation.

Atomic compositions of the samples were analysed by EDS, averaging various (at least three readings) area scans (>100 μm^2) and the results are listed in Table 1. The compositions obtained by the EDS analyses are close to the intended compositions, although further optimisations in the deposition conditions may be required to achieve the target composition particularly for the Zr–Ni alloy. The fabrication of amorphous Zr–Ni alloys (with varying compositions) by magnetron sputtering was previously reported by Coulter and Driscoll [16]. EDS analysis of the deposited samples (Table 1) also suggests that good control of the thin-film composition can be achieved by precise control of the alloying elements deposition rate.

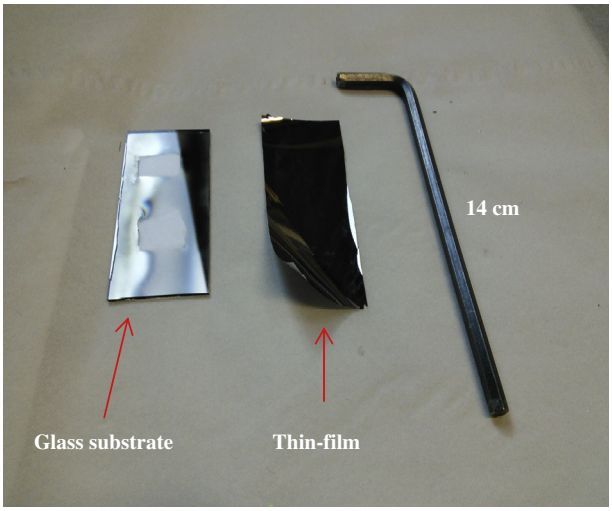

Fig. 1. Magnetron sputtered thin film peeled off the glass substrate.

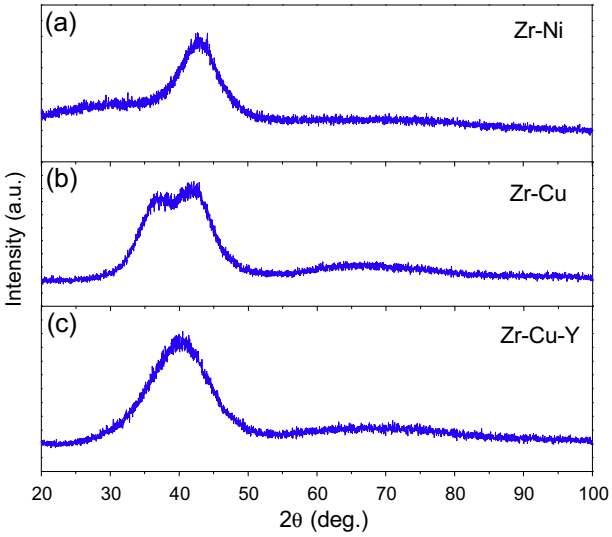

Fig. 2. XRD diffraction patterns of as fabricated (a) Zr–Ni, (b) Zr–Cu and (c) Zr–Cu–Y alloys by magnetron sputtering.

3.2. Surface morphology

The surface topographies of the magnetron sputtered alloys are shown in Fig. 3a–c. SEM images suggest deposition of continuous

Table 1
Sputtering conditions and compositional analyses of the alloys fabricated by magnetron sputtering. The film thicknesses and the activation energies for nucleation and growth (see Fig. 5) of each sample are also listed.

Alloy	Target current (A)				EDS (at.%)	Film thickness (μm)	E_a (kJ/mol)	
	Zr	Cu	Y	Ni			Nucleation	Growth
$Zr_{54}Cu_{46}$	1.42	0.5	–	–	$Zr_{54}Cu_{46}$	5.7	418.7 ± 5.3	395.9 ± 4.3
$Zr_{30}Cu_{60}Y_{10}$	1.25	0.8	0.5	–	$Zr_{30}Cu_{57.5}Y_{12.5}$	5.9	347.2 ± 5.8	415.5 ± 4.5
$Zr_{36}Ni_{64}$	0.76	–	–	0.5	$Zr_{40.5}Ni_{59.5}$	3.5	287.1 ± 3.3	234.5 ± 0.5